Reduced Bone Perfusion in Osteoporosis: Likely Causes in an Ovariectomy Rat Model[1]

James F. Griffith, FRCR
Yi-Xiang J. Wang, MMed, PhD
Hua Zhou, MMed
Wing Hang Kwong, PhD
Wing Tak Wong, BSc
Yan-Lin Sun, MB, PhD
Yu Huang, PhD
David K. W. Yeung, PhD
Ling Qin, PhD
Anil T. Ahuja, FRCR

Purpose: To investigate the cause of reduced vertebral perfusion in a rat ovariectomy model.

Materials and Methods: Experimental protocol was approved by the local Animal Experiment Ethics Committee. Twenty-two Sprague-Dawley rats were studied. Computed tomographic bone densitometry and magnetic resonance perfusion imaging were performed at baseline and 2, 4, and 8 weeks after ovariectomy ($n = 11$) or sham surgery ($n = 11$). Perfusion parameters analyzed were maximum enhancement (E_{max}) and enhancement slope (E_{slope}). After the animals were sacrificed, the aorta and femoral artery were analyzed for vessel reactivity, and the lumbar vertebrae were analyzed for marrow content.

Results: In control rats, bone mineral density (BMD), E_{max}, and E_{slope} remained constant. In ovariectomy rats, a comparable reduction in BMD and the perfusion parameters at two weeks post-ovariectomy (BMD, 9.3%; E_{max}, 11.6%; E_{slope}, 9%) was seen 2 weeks after ovariectomy, and further reductions were seen 4 weeks (BMD, 17.5%; E_{max}, 15.6%; E_{slope}, 33%) and 8 weeks (BMD, 18.8%; E_{max}, 14.2%; E_{slope}, 33%) after ovariectomy. Endothelial dysfunction was observed in both the aorta and femoral artery of the ovariectomy group but not of the control group. Increased marrow fat area was seen in the ovariectomy group (52.9% vs 21.6%; $P < .01$) owing to an increase in fat cell number. Decreased erythropoetic marrow area (32.5% vs 48.6%; $P < .05$) was also observed in the ovariectomy group.

Conclusion: Reduced bone perfusion occurs in synchrony with reduced BMD. The most likely causes of reduced bone perfusion are a reduction in the amount of erythropoetic marrow and endothelial dysfunction after ovariectomy.

Supplemental material: *http://radiology.rsna.org/lookup/suppl/doi:10.1148/radiol.09090608/-/DC1*

[1] From the Departments of Diagnostic Radiology and Organ Imaging (J.F.G., Y.X.J.W., H.Z., Y.L.S., D.K.W.Y., A.T.A.), Anatomy (W.H.K.), Physiology (W.T.W., Y.H.), and Orthopedics and Traumatology (L.Q.), Prince of Wales Hospital, Chinese University of Hong Kong, Shatin, NT, Hong Kong; and Department of Radiology, First Affiliated Hospital, Medical College, Zhejiang University, Hangzhou, Zhejiang Province, China (H.Z.). Received April 15, 2009; revision requested June 5; revision received September 1; final version accepted September 9. Supported by a grant from Research Grants Council of Hong Kong Special Administrative Region, China (project no. 464508). **Address correspondence to** J.F.G. (e-mail: *griffith@cuhk.edu.hk*).

Bone structure and quality are dependent on bone blood flow, cellular metabolism, and structural matrix. Bone perfusion is reduced in osteoporotic bone, but the cause of this reduced perfusion is not clear (1–4). Reduced medullary canal vascularity, including capillary rarefaction, is a feature of senile osteoporosis (5). At a cellular level, hypoxia decreases bone mineralization and stimulates osteoclast activity (6). Some researchers (1,6–9) believe that decreases in osseous vascularity contribute to the increased fracture risk in older individuals. The temporal relationship between reduced bone mineral density (BMD) and reduced perfusion is, however, unknown.

Magnetic resonance (MR) imaging–derived parameters of vertebral marrow blood perfusion have been found to be significantly decreased in osteoporotic subjects (2,3,10). It has been proposed that the decreased bone perfusion in osteoporosis may be due to decreased bone turnover or increased marrow fat content that impedes venous return (2,11). Endothelial dysfunction is another potential cause of impaired bone perfusion in osteoporosis (12,13).

We undertook this longitudinal animal-based study to investigate the cause of reduced bone perfusion in osteoporosis. In particular, we wanted to investigate the temporal relationship between bone perfusion and BMD, as well as the relationship with vascular reactivity and marrow content. Bilateral ovariectomy in the adult female rat is a commonly used model for studying the effects of bone loss (14–16).

Advances in Knowledge

- In an animal model, reduction in bone perfusion occurs in synchrony with a reduction in bone mineral density (BMD).
- Decrease in BMD after ovariectomy is associated with a reduction in the relative amount of erythropoetic marrow.
- Reduction in perfusion associated with decreased BMD after ovariectomy is most likely caused by a combination of reduced erythropoetic marrow and endothelial dysfunction.
- Increase in marrow fat after ovariectomy is owing to an increase in fat cell number.

Materials and Methods

The experimental protocol was approved by the local Animal Experiment Ethics Committee. Twenty-two 6-month-old female Sprague-Dawley rats were used in our study. The animals were housed 2–3 animals per stainless steel cage at 22°C with a 12-hour light-dark cycle and received a standard rat chow diet and water ad libitum. For MR imaging and surgery, rats were anesthetized by using a combination of xylazine (10 mg per kilogram of body weight; Rompun, Bayer HealthCare, Leverkusen, Germany) and ketamine (90 mg/kg; Ketalar, Pfizer, Hong Kong). The number of animals used was selected by considering a power analysis of a pilot study (17) and possible technical failure or animal death during the course of the study.

Computed Tomographic Assessment of Vertebral BMD

Rat lumbar vertebral BMD was measured by using a clinical multidetector computed tomographic (CT) scanner (LightSpeed VCT 64; GE Healthcare, Milwaukee, Wis) with a continuous axial 0.625-mm section thickness. A more detailed description of the method we used to obtain small-animal BMD from a clinical CT scanner has been reported by Wang et al (18). Lumbar vertebral BMD for each rat was defined as the mean BMD of vertebrae L2 through L5. To eliminate any potential effect of retained gadolinium-based contrast agent on bone densitometry, CT was performed prior to MR perfusion studies in all cases.

MR Assessment of Vertebral Bone Perfusion

MR imaging was performed by using a 1.5-T clinical MR imaging system (Intera NT; Philips Medical Systems, Best, the Netherlands) with a maximum gradient strength of 30 mT/m. Rats were anesthetized, and a 24-gauge heparinized catheter was inserted into the tail vein. A surface coil with a diameter of 4.7 cm (Micro 4.7; Philips Medical Systems) was placed under the rat lumbar spine region as the radiofrequency receiver, and the body volume coil was used as the radiofrequency transmitter. Following a coronal scout acquisition, a midsagittal T1-weighted image of the lumbar spine was obtained. A dynamic single-section short T1-weighted gradient-echo MR series (repetition time msec/echo time msec, 4/1.4; flip angle, 15°; section thickness, 5 mm; matrix, 128 × 51; in-plane resolution, 0.625 × 0.625 mm; number of signals acquired, 1; temporal resolution, ~0.6 sec per acquisition) was obtained in the sagittal plane. After 60 baseline images were acquired, a gadolinium-based contrast agent (gadoterate meglumine, Dotarem; Guerbet Group, Roissy, France) was injected into the tail vein (0.3 mmol/kg [ie, 0.15 mL for a 250-g rat]) followed by a 0.5-mL bolus of normal saline (injection time, <1 second). Tail vein catheter placement, contrast agent injection, and normal saline flush were performed by the same operator (Y.X.J.W., with over 7 years experience in small-animal surgery and handling). Dynamic MR imaging took approximately 8 minutes to acquire 800 images.

Published online
10.1148/radiol.09090608

Radiology 2010; 254:739–746

Abbreviations:
BMD = bone mineral density
E_{max} = maximum enhancement
E_{slope} = enhancement slope
L-NAME = nitro-L-arginine methyl ester

Author contributions:
Guarantors of integrity of entire study, J.F.G., L.Q.; study concepts/study design or data acquisition or data analysis/interpretation, all authors; manuscript drafting or manuscript revision for important intellectual content, all authors; approval of final version of submitted manuscript, all authors; literature research, J.F.G., Y.X.J.W., H.Z., Y.L.S., D.K.W.Y., L.Q.; experimental studies, J.F.G., Y.X.J.W., H.Z., W.H.K., W.T.W., Y.L.S., Y.H., D.K.W.Y., L.Q.; statistical analysis, J.F.G., Y.X.J.W., H.Z., W.T.W., Y.H., L.Q.; and manuscript editing, J.F.G., Y.X.J.W., W.T.W., Y.H., D.K.W.Y., L.Q., A.T.A.

Authors stated no financial relationship to disclose.

Dynamic MR images were processed on a workstation (ViewForum; Philips Medical Systems). Regions of interest were drawn over the cancellous part of the lumbar vertebrae from L2 to L5, excluding the vertebral cortex (Fig 1). Signal intensity enhancement over time was recorded and plotted as a time–signal intensity curve. From this time–signal intensity curve, two MR perfusion indexes were analyzed: maximum enhancement (E_{max}) and enhancement slope (E_{slope}). Both relate to the first rapidly rising part of the curve. E_{max} was defined as the maximum percentage increase in signal intensity from baseline and was calculated as follows (2):

$$E_{max} = \left[\frac{(I_{max} - I_{base})}{I_{base}}\right] \cdot 100,$$

Figure 1

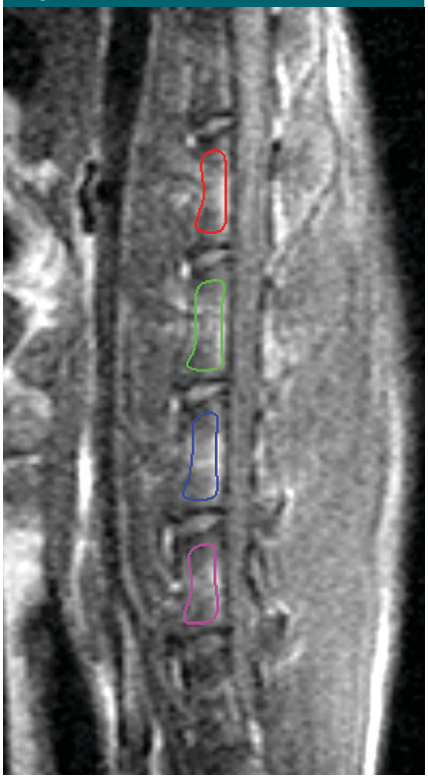

Figure 1: Midsagittal T1-weighted MR image (4/1.4; flip angle, 15°) of a rat lumbar spine show outlined medullary canals of lumbar vertebrae, excluding cortex. Rat lumbar spine has six rather than five vertebral bodies. Red = L2, green = L3, blue = L4, purple = L5.

where I_{max} is the maximum signal intensity of the first rapidly rising part of the time–signal intensity curve and I_{base} is the mean signal intensity of the first 50 images. E_{slope} was defined as the rate of enhancement between 10% and 90% of the maximum signal intensity difference between I_{max} and I_{base}. It was calculated as follows (2):

$$E_{slope} = \left[\frac{0.8 \cdot (I_{max} - I_{base})}{I_{base} \cdot (t_{90\%} - t_{10\%})}\right] \cdot 100,$$

where $t_{10\%}$ and $t_{90\%}$ are the times when signal intensity reaches 10% and 90%, respecitvely, of the signal intensity difference between I_{base} and I_{max}. Data from four lumbar vertebrae (L2 through L5) were obtained, and the mean of these four vertebrae was used as the result for each animal.

Ovariectomy and Sham Surgery

After baseline CT densitometry and MR examination, 11 rats underwent bilateral ovariectomy with a subcostal incision. Ovaries and surrounding fat tissue were removed. Successful ovariectomy was confirmed at necropsy through absence of ovarian tissue and atrophy of uterine horns. The remaining 11 rats underwent sham surgery consisting of exposure of the ovaries but no excision. All surgeries were performed by a single radiologist (Y.X.J.W., with over 7 years experience in small-animal surgery).

Longitudinal CT and MR Assessments of Vertebral BMD and Perfusion

Repeat CT bone densitometry and MR measurement of lumbar vertebral perfusion were performed 2, 4, and 8 weeks after ovariectomy or sham surgery. After week 8 CT and MR imaging, the animals were sacrificed by using a cervical dislocation. The abdominal aorta and right femoral artery were harvested fresh to assess vascular reactivity, and the lumbar vertebrae were harvested for assessment of vertebral marrow content. CT and MR measurements and in vivo animal procedures were performed by two radiologists (Y.X.J.W. and H.Z., with 7 and 3 years experience in animal research, respectively).

Vascular Reactivity Assessment

For vascular reactivity assessment, the aorta and right femoral artery of each rat were dissected and transferred to ice-cold oxygenated Krebs solution for storage. Arteries were dissected free of surrounding connective tissues. Two 3-mm-wide ring segments were cut from each aorta and femoral artery. The endothelium was removed from one ring by gently rubbing the luminal surface with stainless steel wire. The endothelium was left intact on the other ring. Each aortic ring was mounted between two stainless steel wire hooks submerged in an organ bath. Each femoral arterial ring was mounted in a myograph chamber held between two tungsten wires (diameter, 40 μm) in a multimyograph system. Each arterial ring was kept in Krebs solution (pH, 7.2–7.4) at 37°C with 95% O_2 and 5% CO_2. Resting tensions (as determined by length–maximum tension relationship measurements) of 2.5 g and 0.5 g were applied to the aorta and femoral artery, respectively, and 1 hour was allowed for both rings to assume a stable resting tension. To investigate endothelium-dependent relaxation, which is mediated by NO from the endothelium (19), rings with intact endothelium were first contracted by using 1 μmol/L phenylephrine to establish a stable constricted tone, and then acetylcholine was added cumulatively (0.003–10 μmol/L) to the bathing solution to induce relaxation (Fig 2). Relaxation was expressed as percentage reduction in arterial contraction (19). To investigate endothelium-independent relaxation or vascular smooth muscle sensitivity to NO, phenylephrine-constricted rings without endothelium were relaxed by using sodium nitroprusside (0.001–10 μmol/L), an NO donor. Phenylephrine-induced contraction was assessed in both the ovariectomy and control groups, as was the degree to which it was abolished by L-NAME (100 μmol/L). L-NAME inhibits the synthesis of NO from L-arginine (Fig 2) (20,21). Physiologic measurements were performed by an experimental physiologist (W.T.W., with 5 years experience in vessel reactivity research).

Figure 2

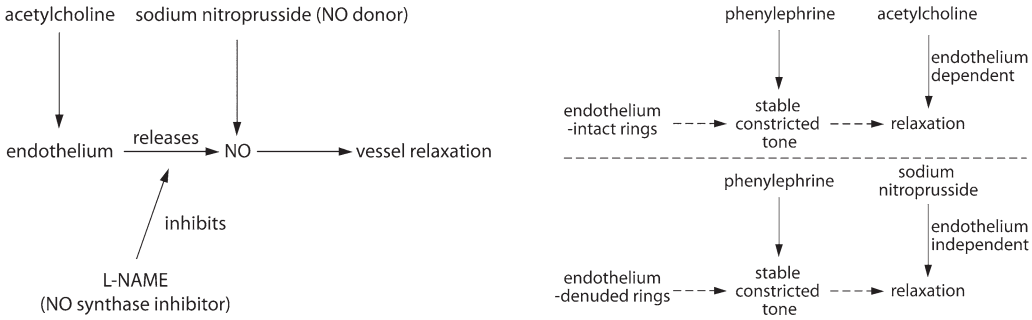

Figure 2: **(a)** Flow diagram shows principle behind vessel reactivity studies. NO is synthesized by endothelium and results in arterial relaxation. Acetylcholine acts as a substrate or stimulates this endothelial release. Sodium nitroprusside provides a direct source of NO. Nitro-L-arginine methyl ester *(L-NAME)* inhibits release of NO. **(b)** Flow diagram of vessel reactivity studies in rings (top) with and (bottom) without endothelium. Phenylephine acts on vascular smooth muscle to induce contraction. If endothelium is functioning normally, acetylcholine will induce relaxation. If endothelium is not functioning properly, sodium nitroprusside can, by providing a direct source of NO, induce relaxation.

Rats Available for Analysis

Evaluation	Baseline	Week 2*	Week 4	Week 8
BMD measurement				
Control group	11	6	11	10
Ovariectomy group	11	5	8	7
Bone perfusion measurement				
Control group	11	6	10	10
Ovariectomy group	11	5	8	7
Myographic and histologic assessment†				
Control group	…	…	…	10
Ovariectomy group	…	…	…	7

Note.—Data are numbers of rats examined at each time. Five of 22 rats died owing to surgery, anesthesia, or infection.

* Availability of MR time limited the number of rats examined during week 2.

† Vascular reactivity studies obtained for six rats in each group.

Histologic Assessment of Vertebral Marrow Cavity

For histologic examination, the excised lumbar spine was fixed in 10% buffered formalin for 3 days and then decalcified with 10% formic acid for 4 weeks. Decalcified samples were embedded in paraffin and cut into 6-mm-thick axial slices. Slices were stained with hematoxylin-eosin. Four vertebral slices from each of the four vertebrae (L2 through L5) were randomly selected for evaluation (magnification, ×200), yielding a total of 16 slices analyzed from each rat. Percentage area of marrow fat, trabecular bone, and erythropoetic marrow was measured in each histologic slice by using image processing software (Image-Pro Plus, version 5.1; Media Cybernetics, Bethesda, Md). The mean of all fields measured from each animal was used for statistical analysis. Histologic analysis was performed by a pathologist (Y.L.S., with 5 years experience).

Statistical Analysis

CT, MR imaging, and histologic data were expressed as means ± standard deviations, while vascular reactivity data were expressed as means ± standard errors of the means. All statistical analyses were performed with software (SPSS, version 14.0; SPSS, Chicago, Ill). One-way analysis of variance for repeated measures was used for longitudinal measure of the same group animals, when significant. Mann-Whitney *U* test was used for nonpaired comparisons, and Wilcoxon signed rank test was used for paired comparisons. All statistical tests were two-sided. A *P* value less than .05 was considered to indicate a significant difference.

Results

One rat died during ovariectomy, and four rats died during the course of the study owing to anesthesia or infection. The total number of rats available for analysis at various time points is shown in the Table.

Vertebral BMD

BMD measurement are shown in Figure 3. BMDs remained consistent in the control rats, with no significant difference seen over the four time points ($P > .05$). In the ovariectomy rats, BMD decreased significantly from baseline at weeks 2 (9.3%, $P = .043$), 4 (17.5%, $P < .001$), and 8 (18.8%, $P < .001$). The difference between weeks 4 and 8 was not significant ($P = .536$).

Vertebral Bone Perfusion

At baseline, there was no difference in E_{max} ($P = .71$) or E_{slope} ($P = .8$) between control and ovariectomy rats. In control

Figure 3

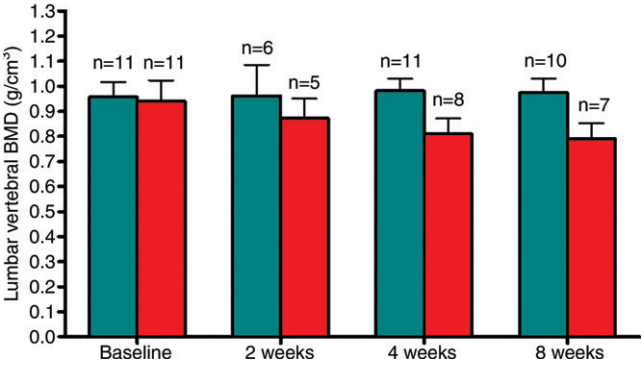

Figure 3: Bar graph shows rat lumbar vertebral BMD at various times in control (teal) and ovariectomy (red) groups. In control rats, BMD remained constant. In ovariectomy rats, BMD started to decrease by week 2 and further decreased by weeks 4 and 8. Bars = standard deviations .

Figure 5

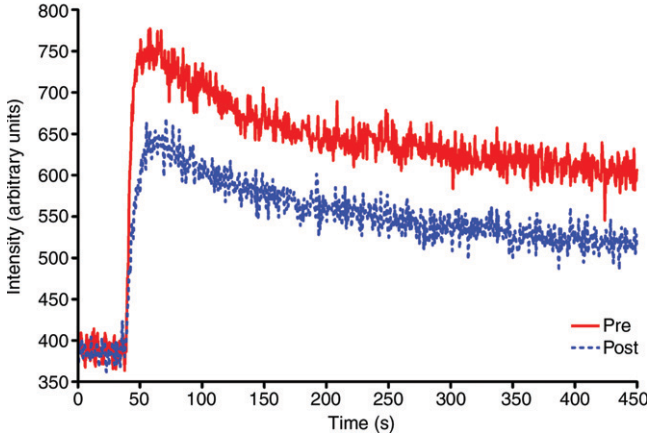

Figure 5: An example of time–signal intensity enhancement curves at baseline *(Pre)* and week 4 *(Post)* in L3 of an ovariectomy rat. Compared with baseline curve, week 4 curve shows reduced E_{max} and a less steep E_{slope}.

Figure 4

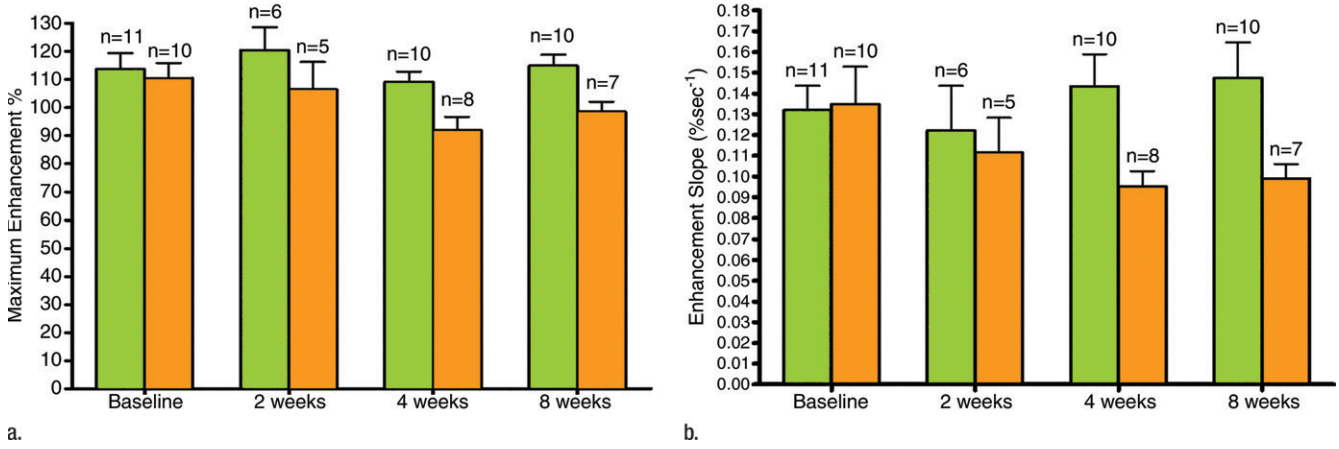

Figure 4: Bar graphs show MR imaging perfusion indexes **(a)** E_{max} and **(b)** E_{slope} at various times in control (green) and ovariectomy (orange) groups. Data are mean measurements obtained from four lumbar vertebrae in each rat from a single-section acquisition. For control rats, E_{max} and E_{slope} remained constant. In ovariectomy rats, E_{max} and E_{slope} started to decrease by week 2 and further decreased by week 4. No significant difference was present between weeks 4 and 8.

rats, both E_{max} and E_{slope} remained stable during the course of the study ($P > .05$) (Fig 4). At week 2, E_{max} in the ovariectomy group was 11.6% less than that in the control group, and E_{slope} was 9% less than that in the control group. These differences did not reach statistical significance ($P = .31$ and .54, respectively) (Fig 4). At week 4, E_{max} in the ovariectomy group was 15.6% less than that in the control group ($P = .027$), and E_{slope} was 33.6% less than that in the control group ($P = .03$) (Figs 4 and 5). At week 8, E_{max} in the ovariectomy group was 14.2% less than that in the control group ($P = .02$), and E_{slope} was 32.9% less than that in the control group ($P = .01$) (Fig 4). No significant differences were present for either E_{max} or E_{slope} between weeks 4 and 8 in the ovariectomy group.

Vascular Reactivity

Acetylcholine-mediated endothelium-dependent relaxation in phenylephrine-constricted aortic and femoral arterial rings was impaired in ovariectomy group as compared with the control group (Fig 6a). Endothelium-independent relaxation by sodium nitroprusside, an NO donor, was comparable between the two groups (Fig 6b). Phenylephrine-induced contraction was greater in the ovariectomy group than in the control group (Fig 6c); this discrepancy was abolished in the presence of L-NAME, an NO synthase inhibitor (Fig 6d, Table E1 [online]).

Histologic Assessment of Vertebral Marrow Cavity

In the control group, marrow fat cell area was 21.6% ± 4.2%, bone trabecular

Figure 6

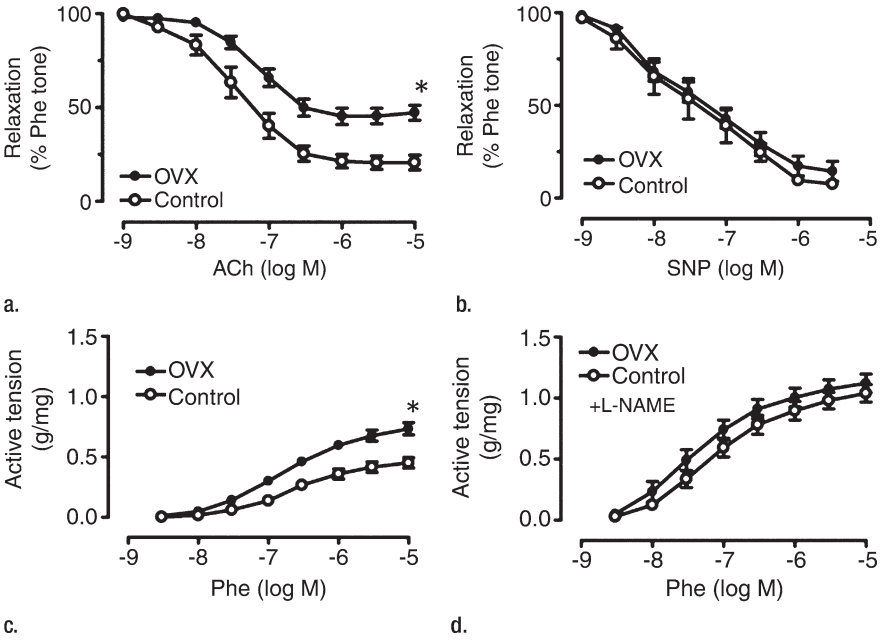

Figure 6: Graphs of vascular reactivity data in aortic rings for ovariectomy *(OVX)* and control groups. **(a)** Acetylcholine *(ACh)*-mediated endothelium-dependent relaxation in phenylephrine *(Phe)*-constricted aortic rings was significantly impaired in ovariectomy versus control group (* = $P < .05$). **(b)** Endothelium-independent vasodilatation by sodium nitroprusside *(SNP)* was comparable between groups. **(c)** Phenylephrine-induced contraction was significantly greater in ovariectomy versus control group (* = $P < .05$). **(d)** This effect was abolished when L-NAME was added. Only results for aortic ring are shown because similar results were observed in femoral rings. Bars = standard errors of means, *log M* = logarithmic transformation of moles per liter, *% Phe tone* = percentage of tension with phenylephrine contraction.

Figure 7

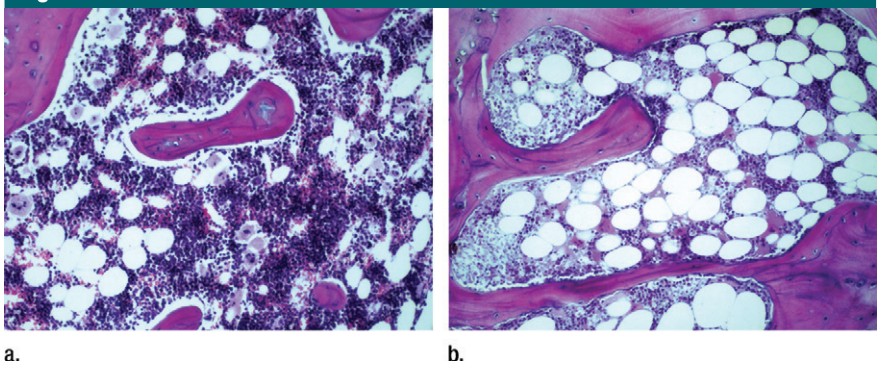

Figure 7: Representative histopathologic slices of lumbar vertebral body medullary canal in **(a)** control and **(b)** ovariectomy rats. Ovariectomy rat had more fat cells in intertrabecular space and a reduced amount of erythropoetic marrow compared with control rat. (Hematoxylin-eosin stain; original magnification, ×200.)

area was 29.8% ± 3.9%, and erythropoetic marrow area was 48.6% ± 4.5%. In the ovariectomy group, marrow fat cell area was 52.9% ± 4.6% ($P < .01$ vs control group), bone trabecular area was 14.6% ± 3.7% ($P < .01$), and erythropoetic marrow area was 32.5% ± 4.8% ($P < .05$) (Fig 7). In other words, the increase in fat cell area in the ovariectomy rats was accompanied not just by a reduction in the amount of trabecular bone but also by a decrease in the amount of erythropoetic marrow.

The fat cell (adipocyte) number in the control group was 39 ± 5 per field (magnification, ×200), while it was 92 ± 6 per field in the ovariectomy group. Therefore, the increase in fat cell area by a factor of 2.45 (52.9% vs 21.6%) in the ovariectomy group was accompanied by a corresponding increase in fat cell number by a factor of 2.35 (92 vs 39). This indicates that the increase in fat in the marrow space that accompanies ovariectomy is mostly owing to an increase in fat cell number rather than an increase in individual fat cell size (Fig 7).

Discussion

Findings in several cross-sectional clinical studies have indicated that perfusion is reduced in osteoporotic bone (1–3,10). This reduction in perfusion affects only bone and not adjacent musculature with the same arterial supply, indicating that reduced perfusion is most likely an intraosseous phenomenon rather than a symptom of more generalized circulatory impairment (3). The primary aim of our study was to investigate the cause of reduced bone perfusion in reduced BMD, particularly the temporal relationship between bone perfusion and BMD, as well as the relationship with vascular reactivity and marrow content.

As expected, sex hormone deficiency led to a reduction in vertebral BMD. At the first assessment with CT and MR 2 weeks after ovariectomy, a comparable reduction in both vertebral BMD and perfusion parameters was observed. Further reduction in both parameters was seen 4 weeks after ovariectomy and again 8 weeks after ovariectomy. At week 2, reductions in BMD and both perfusion parameters by a factor of about 10% were observed. It is our belief that reduced bone perfusion occurs concurrently with a reduction in BMD.

We also investigated the relationship between bone perfusion and vascular reactivity because clinical studies have shown how endothelial dysfunction is

related osteoporosis (12,13). Ovariectomy-induced endothelial dysfunction is known to occur in the aorta, but this effect has not been previously demonstrated in the femoral arteries (19,22). NO is produced by the endothelium and is known as the "endothelium-derived relaxing factor." Endothelial-released NO signals downstream vascular smooth muscle to relax, resulting in vasodilatation, increased blood flow, and, as a result, improved contrast enhancement.

Endothelial dysfunction resulting from decreased NO bioavailability was observed in the aorta and femoral artery in the ovariectomy group but not in the control group. Endothelium-dependent relaxation, mediated by NO, was impaired in ovariectomy rats, while endothelium-independent relaxation with sodium nitroprusside was similar in both ovariectomy and control groups. This indicates that endothelial release of NO was impaired, but the sensitivity of vascular smooth muscle to NO was not altered. Furthermore, the observed enhanced contraction with phenylephrine seen in ovariectomy rats was abolished by L-NAME, an NO synthase inhibitor, indicating a decrease in NO availability owing to endothelial dysfunction.

Therefore, our findings demonstrate that endothelial dysfunction as a result of reduced NO availability occurs after ovariectomy. This endothelial dysfunction could, through impaired vasodilatation or enhanced vascular tone, lead to reduced blood flow and may be a cause of the reduced perfusion seen with reduced BMD. Our results are supported by those of Prisby et al (9), who, by using radiolabeled microspheres, demonstrated a 21% reduction in metaphyseal blood flow in old rats compared with young rats. This reduction in blood flow was associated with impaired endothelium-dependent vasodilatation and decreased NO bioavailability (9).

Decreased release of endothelium-derived substances, such as NO or prostacyclin, is of particular interest in osteoporosis as both NO and prostacylcin have a potential downstream effect of promoting bone formation and limiting resorption (23). Endothelial dysfunction is not likely, however, to be the sole cause of reduced bone perfusion in the presence of reduced BMD since the effects of endothelial dysfunction are more likely to be systemic with the aorta and femoral artery seen to be equally affected in our study.

Another possible cause of reduced bone after ovariectomy is an alteration in marrow content, as shown in our study. The medullary cavity is composed mainly of marrow fat, trabecular bone, and erythropoetic marrow, with a small component occupied by vascular channels (arterioles, venules, and capillary sinusoids). Within the confined space of the vertebral body, an increase in one component can only occur at the expense of another component (11). Clinical MR spectroscopic studies have shown that as BMD decreases there is a reciprocal increase in marrow fat content (2,3). The rat vertebral body is too small to allow proton MR spectroscopy at 1.5 T, but we were able to study the effect of ovariectomy on marrow content histologically. Following ovariectomy, increased marrow fat area of 31.3% was observed secondary to an increase in fat cell number rather than fat cell size. This increased fat cell number may be the result of mesenchymal stem cell differentiation switching more toward adipocytosis rather than osteoblastogenesis (24,25).

The relative increase in marrow fat area was coincident not just with a reduction in the amount of trabecular bone, which decreased by 15.2%, but also with a reduction in the amount of erythropoetic marrow, which decreased by 16.1%. This reduction is erythropoetic marrow may be akin to "senile anemia" (26–29). Both the increase in marrow fat and the decrease in erythropoetic marrow may be related to estrogen depletion given that the postmenopausal state is recognized to be associated with increases in both body mass and anemia, the latter of which may be associated with a relatively hypoplastic marrow, though this, to our knowledge, has not been specifically investigated (30,31). It appears, therefore, that the increase in fat content after ovariectomy is not simply due to fat occupying the space vacated by trabecular bone and erythropoetic marrow. Results of a preliminary positron emission tomographic study (32) have indicated that the metabolic activity of erythropoetic marrow is up to six times greater than that of fatty marrow. Overall, it seems somewhat likely that this erythropoetic marrow may be accounting for the reduced bone perfusion seen accompanying reduced BMD.

We investigated longitudinal changes in bone perfusion, vascular reactivity, and marrow content in relationship to BMD. Our study cohort was small, and our findings need to be validated in larger preclinical and clinical studies. More in-depth MR-based perfusion models (33,34) would help to provide information on specific elements of perfusion (eg, arterial input and permeability), while means of determining endothelial function on MR images need to be explored (35). Clinical MR-based studies (3,11) have focused more on quantification of fatty rather than erythropoetic marrow owing to difficulty in accurately quantifying erythropoetic marrow. Means of noninvasively quantifying this metabolically active element of marrow tissue requires further study.

Practical applications: Bone loss after ovariectomy is associated not just with a reduction in bone perfusion and an increase in marrow fat, but also, more importantly, with a decrease in the amount of functioning marrow. Because bone loss does not occur in isolation, a more encompassing paradigm, with consideration given to perfusion, red and fatty marrow, and BMD, may best serve future osteoporotic research.

In conclusion, the results of our animal study show that reduced bone perfusion occurs in synchrony with reduced BMD and is most likely the result of a reduction in the amount of erythropoetic marrow and impaired endothelial function after ovariectomy. This decrease in erythropoetic marrow accompanies an increase in marrow fat, which occurs as a result of an increase in fat cell number rather than size.

Acknowledgments: The authors thank the radiographers at the Prince of Wales Hospital for MR imaging data acquisition and Gang Wang, MB, for histologic processing.

References

1. Shih TT, Liu HW, Chang CJ, Wei SY, Shen LC, Yang PC. Correlation of MR lumbar bone marrow perfusion with bone mineral density in female subjects. Radiology 2004;233:121–128.
2. Griffith JF, Yeung DK, Antonio GE, Wong SY, Lau EM, Leung PC. Vertebral bone mineral density, marrow perfusion, and fat content in healthy men and men with osteoporosis: dynamic contrast-enhanced MR imaging and MR spectroscopy. Radiology 2005;236:945–951.
3. Griffith JF, Yeung DK, Antonio GE, et al. Vertebral marrow fat content and diffusion and perfusion indexes in women with varying bone density: MR evaluation. Radiology 2006;241:831–838.
4. Wang YX, Griffith JF, Kwok AW, et al. Differential decrease of blood perfusion among femoral head, femoral neck and femoral shaft in patients with osteoponia and osteoporosis. Bone 2009;45:711–715.
5. Burkhardt R, Kettner G, Bohm W, et al. Changes in trabecular bone, hematopoiesis and bone-marrow vessels in aplastic-anemia, primary osteoporosis, and old-age: a comparative histomorphometric study. Bone 1987;8:157–164.
6. Utting JC, Robins SP, Brandao-Burch A, Orriss IR, Behar J, Arnett TR. Hypoxia inhibits the growth, differentiation and bone-forming capacity of rat osteoblasts. Exp Cell Res 2006;312:1693–1702.
7. Bloomfield SA, Hogan HA, Delp MD. Decreases in bone blood flow and bone material properties in aging Fischer-344 rats. Clin Orthop Relat Res 2002;396:248–257.
8. Kita K, Kawai K, Hirohata K. Changes in bone marrow blood flow with aging. J Orthop Res 1987;5:569–575.
9. Prisby RD, Ramsey MW, Behnke BJ, et al. Aging reduces skeletal blood flow, endothelium-dependent vasodilation and nitric oxide bioavailability in rats. J Bone Miner Res 2007;22:1280–1288.
10. Griffith JF, Yeung DK, Tsang PH, et al. Compromised bone marrow perfusion in osteoporosis. J Bone Miner Res 2008;23:1068–1075.
11. Schellinger D, Lin CS, Lim J, Hatipoglu HG, Pezzullo JC, Singer AJ. Bone marrow fat and bone mineral density on proton MR spectroscopy and dual-energy X-ray absorptiometry: their ratio as a new indicator of bone weakening. AJR Am J Roentgenol 2004;183:1761–1765.
12. Sanada M, Taguchi A, Higashi Y, et al. Forearm endothelial function and bone mineral loss in postmenopausal women. Atherosclerosis 2004;176:387–392.
13. Sumino H, Ichikawa S, Kasama S, et al. Relationship between brachial arterial endothelial function and lumbar spine bone mineral density in postmenopausal women. Circ J 2007;71:1555–1559.
14. Jee WS, Yao W. Overview: animal models of osteopenia and osteoporosis. J Musculoskelet Neuronal Interact 2001;1:193–207.
15. Liu XQ, Chen HY, Tian XY, Setterberg RB, Li M, Jee WS. Alfacalcidol treatment increases bone mass from anticatabolic and anabolic effects on cancellous and cortical bone in intact female rats. J Bone Miner Metab 2008;26:425–435.
16. Lelovas PP, Xanthos TT, Thoma SE, Lyritis GP, Dontas IA. The laboratory rat as an animal model for osteoporosis research. Comp Med 2008;58:424–430.
17. Wang YX, Griffith JF, Yeung DK, Zhou H, Zhang YF, Qin L. Decease of vertebra bone mineral density is associated with decease of vertebra blood perfusion: dynamic contrast enhanced MRI study in rat ovariectomy model [poster]. Presented at the 54th annual meeting of the Orthopaedic Research Society, San Francisco, Calif, March 2–5, 2008.
18. Wang YX, Griffith JF, Zhou H, et al. Rat lumbar vertebrae bone densitometry using multidetector CT. Eur Radiol 2009;19:882–890.
19. Wong CM, Yung LM, Leung FP, et al. Raloxifene protects endothelial cell function against oxidative stress. Br J Pharmacol 2008;155:326–334.
20. Palmer RM, Ashton DS, Moncada S. Vascular endothelial cells synthesize nitric oxide from L-arginine. Nature 1988;333:664–666.
21. Rees DD, Palmer RM, Hodson HF, Moncada S. A specific inhibitor of nitric oxide formation from L-arginine attenuates endothelium-dependent relaxation. Br J Pharmacol 1989;96:418–424.
22. Taddei S, Virdis A, Ghiadoni L, et al. Menopause is associated with endothelial dysfunction in women. Hypertension 1996;28:576–582.
23. Samuels A, Perry MJ, Gibson RL, Colley S, Tobias JH. Role of endothelial nitric oxide synthase in estrogen-induced osteogenesis. Bone 2001;29:24–29.
24. Duque G. Bone and fat connection in aging bone. Curr Opin Rheumatol 2008;20:429–434.
25. Rosen CJ, Bouxsein ML. Mechanisms of disease: is osteoporosis the obesity of bone? Nat Clin Pract Rheumatol 2006;2:35–43.
26. Takasaki M, Tsurumi N, Harada M, Rokugo N, Ebihara Y, Wakasugi K. Changes of bone marrow arteries with aging [in Japanese]. Nippon Ronen Igakkai Zasshi 1999;36:638–643.
27. Justesen J, Stenderup K, Ebbesen EN, Mosekilde L, Steiniche T, Kassem M. Adipocyte tissue volume in bone marrow is increased with aging and in patients with osteoporosis. Biogerontology 2001;2:165–171.
28. Verma S, Rajaratnam JH, Denton J, Hoyland JA, Byers RJ. Adipocytic proportion of bone marrow is inversely related to bone formation in osteoporosis. J Clin Pathol 2002;55:693–698.
29. Steiniche T. Bone histomorphometry in the pathophysiological evaluation of primary and secondary osteoporosis and various treatment modalities. APMIS Suppl 1995;51:1–44.
30. Hartsock RJ, Smith EB, Petty CS. Normal variations with aging of the amount of hematopoetic tissue in bone marrow from the anterior iliac crest: a study made from 177 cases of sudden death examined by necropsy. Am J Clin Pathol 1965;43:326–331.
31. Chahal HS, Drake WM. The endocrine system and ageing. J Pathol 2007;211:173–180.
32. Basu S, Houseni M, Bural G, et al. Magnetic resonance imaging based bone marrow segmentation for quantitative calculation of pure red marrow metabolism using 2-deoxy-2-[F-18] fluoro-D-glucose-positron emission tomography: a novel application with significant implications for combined structure-function approach. Mol Imaging Biol 2007;9:361–365.
33. Tofts PS. Modeling tracer kinetics in dynamic Gd-DTPA MR imaging. J Magn Reson Imaging 1997;7:91–101.
34. Brix G, Semmler W, Port R, Schad LR, Layer G, Lorenz WJ. Pharmacokinetic parameters in CNS Gd-DTPA enhanced MR imaging. J Comput Assist Tomogr 1991;15:621–628.
35. Ghiadoni L, Versari D, Giannarelli C, Faita F, Taddei S. Non-invasive diagnostic tools for investigating endothelial dysfunction. Curr Pharm Des 2008;14:3715–3722.